Modulation of σ-Alkane Interactions in [Rh(L2)(alkane)]$^+$ Solid-State Organometallic (SMOM) Systems by Variation of the Chelating Phosphine and Alkane: Access to η^2,η^2-σ-Alkane Rh(I), η^1-σ-Alkane Rh(III) Complexes, and Alkane Encapsulation.

Antonio J. Martínez-Martínez,[a] Bengt E. Tegner,[b] Alasdair I. McKay,[a] Alexander J. Bukvic,[a] Nicholas H. Rees,[a] Graham J. Tizzard,[c] Simon J. Coles,[c] Mark R. Warren,[d] Stuart A. Macgregor*[b] and Andrew S. Weller*[a]

[a] Chemistry Research Laboratories, University of Oxford, Oxford OX1 3TA, United Kingdom

[b] Institute of Chemical Sciences, Heriot Watt University, Edinburgh EH14 4AS, United Kingdom

[c] UK National Crystallography Service, Chemistry, Faculty of Natural and Environmental Sciences, University of Southampton. Southampton, SO17 1BJ, United Kingdom

[d] Diamond Light Source Ltd., Harwell Science and Innovation Campus, Didcot, OX11 0DE. United Kingdom

ABSTRACT: Solid/gas Single–Crystal to Single–Crystal (SC–SC) hydrogenation of appropriate diene precursors forms the corresponding σ–alkane complexes [Rh(Cy$_2$P(CH$_2$)$_n$PCy$_2$)(L)][BAr$^F{}_4$] (n = 3, 4) and [RhH(Cy$_2$P(CH$_2$)$_2$(CH)(CH$_2$)$_2$PCy$_2$)(L)][BAr$^F{}_4$] (n = 5, L = norbornane, NBA; cyclooctane, COA). Their structures, as determined by single–crystal X-ray diffraction, have cations with Rh···H–C σ–interactions that are modulated by both the chelating ligand and the identity of the alkane, while all sit in an octahedral anion–microenvironment. These complexes and their bonding are also interrogated using periodic DFT, QTAIM, NBO calculations, variable temperature solid–state NMR spectroscopy and HETCOR and Non–Quaternary Suppression experiments. With NBA as the alkane ligand, the bite angle of the phosphine has little effect, forming [Rh(Cy$_2$~~P(CH$_2$)$_n$PCy$_2$)(~~$\eta^2\eta^2$–NBA)][BAr$^F{}_4$], for n = 3 and 4, structures of which show a chelating bidentate σ–alkane complexes with η^2 Rh···H–C 3c–2e interactions. For n = 5 phosphine backbone C–H ac~~tivation occurs~~ to form [RhH(Cy$_2$P(CH$_2$)$_2$(CH)(CH$_2$)$_2$PCy$_2$)(η–NBA)][BAr$^F{}_4$], which shows a significant long range disorder. A well–defined CH$_2$Cl$_2$ adduct forms by displacement of the alkane in solution, [Rh(Cy$_2$P(CH$_2$)$_2$(CH)(CH$_2$)$_2$PCy$_2$)H(κ^1–ClCH$_2$Cl)][BAr$^F{}_4$], that has been characterized crystallographically. Variable temperature solution NMR and DFT calculations also show backbone C–H activation is reversible on the NMR timescale at 298 K. With the COA alkane ligand different structures are accessed. For n = 3 addition of H$_2$ to the COD precursor forms [Rh(Cy$_2$P(CH$_2$)$_3$PCy$_2$)][COA⊂BAr$^F{}_4$] in which the COA is not ligated with the metal but is encapsulated in the octahedral anion–microenvironment, and the metal center forms two intramolecular agostic η^1 Rh···H–C interactions with the phosphine cyclohexyl groups. For n = 4 no stable complex could be isolated. For n = 5, phosphine backbone C–H activation occurs to form [RhH(Cy$_2$P(CH$_2$)$_2$(CH)(CH$_2$)$_2$PCy$_2$)(η^1–COA)][BAr$^F{}_4$], and a well–defined structure shows that the alkane ligand is interacting with the metal center through an end-on η^1 Rh···H–C interaction, the first example of such a structure characterized crystallographically in the solid state. As for the NBA complex this can be trapped by addition of CH$_2$Cl$_2$. These studies show the power of Solid–State Organometallic Chemistry (SMOM) when combined with periodic DFT calculations to provide access to, and characterize, a range of different σ–alkane M···H–C coordination motifs by systematic variation of the ligand set: ranging from chelating η^2,η^2 Rh···H–C, through to more weakly bound η^1 Rh··H–C and ultimately to systems where the alkane is not ligated with the metal center, but sits encapsulated in the supporting anion microenvironment. The importance of dispersive non–covalent interactions in stabilizing these different motifs in the solid–state is also highlighted.

1. Introduction. The ability to tune the local environment around a metal center by variation of supporting ligands is an important concept widely used in homogenous organometallic synthesis and catalysis.[1,2] A well–documented example of this comes from bidentate phosphine ML$_2$–type complexes,[3,4] as by altering the L–M–L bite angle and substitution at phosphine the resulting steric (e.g. the solid–cone angle, Θ[5]), or electronic (e.g. oxidation state[6] or degree of bond activation[7]), changes ultimately can provide the ability to control structure, speciation and, through the energetics of elementary reaction steps in catalysis, activity and selectivity.

Extending such concepts to heterogeneous systems is difficult given the resulting challenges associated with precisely defining single–site active centers and their extended coordination environments.[8] While chelating phosphine complexes supported by metal organic frameworks,[9] porous coordination polymers,[10] nanoparticles,[11] mesoporous–hosts[12] and silica–surfaces[13] have been reported, the role of the chelating ligand in determining structure and reactivity is less well–developed. Nevertheless, precise control of well–defined, and reactive, metal centers in heterogeneous systems could lead to enhanced activity and selectivity in catalysis, as frequently demonstrated in homogenous processes.[1,4]

We have recently shown that single–crystal to single–crystal (SC–SC) solid/gas reactions between H_2 and the appropriate $[\mathrm{RhL_2(diene)}]^+$ precursors forms well–defined but reactive σ–alkane[14-16] complexes directly in the solid–state, *e.g.* $[\mathrm{Rh(Cy_2P(CH_2)_2PCy_2)(\eta^2\eta^2\text{–}NBA)}][\mathrm{BAr^F{}_4}]$, **[1–NBA][BAr$^F{}_4$]** (NBA = norbornane, $\mathrm{Ar^F}$ = 3,5–$\mathrm{(CF_3)_2C_6H_3}$), Fig. 1B).[17-20] Such σ–complexes contain 3–center 2–electron (3c-2e) Rh⋯H–C bonds,[21,22] and are of general interest from the fundamental challenges presented by their synthesis and characterization,[14,15] as well as their central role as intermediates in C–H activation processes.[23-26] When prepared in this way these σ–alkane complexes show remarkable relative stability compared with species prepared by solution routes; the latter are generally characterized in situ using NMR spectroscopy, on small scale (2–20 mg) at very low temperature and have limited lifetimes even under these relatively constrained conditions.[27-31]

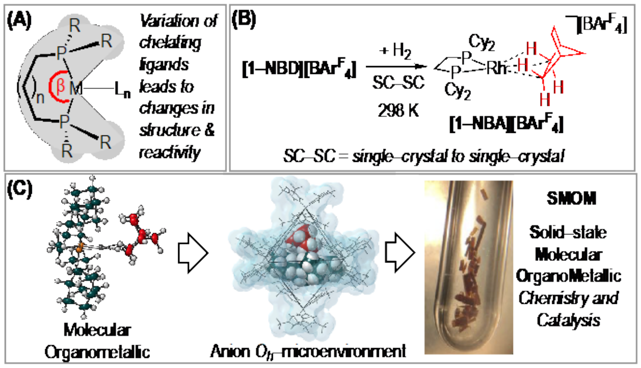

Figure 1. **(A)** Control of local environment in {ML$_2$} complexes: Bite angle = β. **(B)** Synthesis of the σ–alkane complex **[1-NBA][BAr$^F{}_4$]**; NBD = norbornadiene. **(C)** The SMOM concept.

This stability in the solid–state originates from the $[\mathrm{BAr^F{}_4}]^-$ anions providing a robust, octahedral, crystalline microenviroment,[32] that allows for isolation, characterization and onward reactivity of the encapsulated organometallic cation to be studied in detail (Fig. 1C).[26,33] These so–called[33] Solid–state Molecular Organometallic (SMOM) systems are related to Supported Organometallic Catalysts (SOMC),[13] Single–Site Heterogeneous Catalysts (SSHC),[34] and MOF–functionalized organometallics,[9,35-37] but, in contrast to these, are not supported by a platform material. Moreover, SMOM systems have the desirable properties of being readily studied at the molecular–level by single–crystal X–ray diffraction, Solid–State NMR (SSNMR) spectroscopy and computational techniques such as periodic DFT.

Scheme 1. Precursor diene complexes used in this study and SC-SC SMOM–synthesis of σ–complexes.

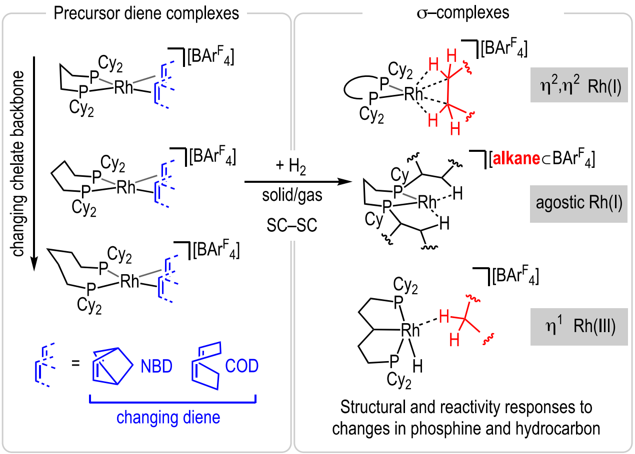

We now report that systematic variation of the P–Rh–P bite angle coupled with the identity of the diene in SMOM systems based upon precursors $[\mathrm{Rh(Cy_2P(CH_2)_nPCy_2)(diene)}][\mathrm{BAr^F{}_4}]$ (n = 3 to 5, diene = norbornadiene, NBD, or 1,5–cyclooctadiene, COD, Scheme 1) results in significant changes in structure and reactivity on addition of H_2 in SC–SC reactions. This results in crystallographically characterized σ–alkane complexes that show markedly different degrees of Rh⋯H–C interaction in response to the changes in *both* phosphine and the precursor diene, while stabilized in the microenvironment provided by the octahedral arrangement of $[\mathrm{BAr^F{}_4}]^-$ anions: these range from chelating η^2,η^2 Rh⋯H–C, through to more weakly bound η^1 Rh⋯H–C and ultimately to systems where the alkane is not ligated with the metal center, but sits encapsulated in the anion framework.

2. Results and Discussion

2.1 Precursor diene complexes.

Precursor complexes of the general formula $[\mathrm{Rh(Cy_2P(CH_2)_nPCy_2)(diene)}][\mathrm{BAr^F{}_4}]$ (diene = NBD or COD) were prepared in which the phosphine and diene are systematically varied: n = 3, **[2–diene][BAr$^F{}_4$]**; n = 4, **[3–diene][BAr$^F{}_4$]**; n = 5, **[4–diene][BAr$^F{}_4$]** (Scheme 2). These are conveniently prepared by reaction of $[\mathrm{Rh(COD)_2}][\mathrm{BAr^F{}_4}]$ with $\mathrm{Cy_2P(CH_2)_nPCy_2}$ to give $[\mathrm{Rh(Cy_2P(CH_2)_nPCy_2)(COD)}][\mathrm{BAr^F{}_4}]$, followed by addition of H_2/1,2–$\mathrm{F_2C_6H_4}$/NBD to give $[\mathrm{Rh(Cy_2P(CH_2)_nPCy_2)(NBD)}][\mathrm{BAr^F{}_4}]$ via *in situ* formation of difluorobenzene-bound[38] intermediates $[\mathrm{Rh(Cy_2P(CH_2)_nPCy_2)(1,2\text{–}F_2C_6H_4)}][\mathrm{BAr^F{}_4}]$. Both COD and NBD precursors were isolated in good (~80%) yield after recrystallization from $\mathrm{CH_2Cl_2}$/pentane. Complexes **[1–diene][BAr$^F{}_4$]** (n = 2) have previously been reported.[18]

These precursor complexes have been characterized by solution NMR spectroscopy and single–crystal X-ray diffraction, which show an O_h arrangement of $[\mathrm{BAr^F{}_4}]^-$ anions surrounding the organometallic cations, as observed for **[1–NBA][BAr$^F{}_4$]**[18] and related complexes.[17,20] The Supporting Materials detail their structures. For the NBD precursors, this homologous series allows for the bite–angle (β) of the various diphosphines in this environment to be compared. Unsurprisingly,[4] β becomes progressively larger with increasing number of methylene units in the chelate backbone (Scheme 2B). The same trend, albeit interestingly with slightly smaller β-angles, is apparent for the COD precursors. With these complexes in hand a systematic study of solid/gas hydrogenation was undertaken.

Scheme 2. (A) Synthesis of diene precursors and (B) representative P-Rh-P bite angles (β) taken from diene structures.[17,39]

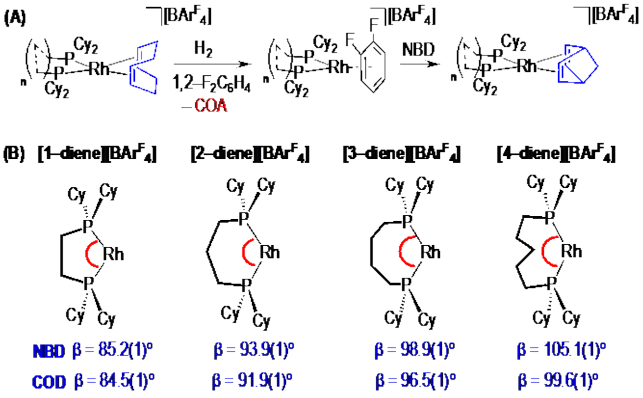

2.2 Hydrogenation of $\{Rh(Cy_2P(CH_2)_2PCy_2)\}^+$/COD.

As previously reported, hydrogenation of **[1-NBD][BAr$^F_4$]** gives **[1-NBA][BAr$^F_4$]** in a rapid (less than 10 mins) SC-SC transformation (see Figure 1B). Here, use of **[1-COD][BAr$^F_4$]** results a slower [40,41] reaction with H_2 (3 hrs) and loss of crystallinity. Dissolving the resulting solid in CD_2Cl_2 afforded the previously-reported zwitterion $[Rh(Cy_2P(CH_2)_2PCy_2)\{(\eta\text{-}C_6H_3(CF_3)_2)BAr^F_3\}]$, **[1-BAr$^F_4$]** and free COA.[18]

2.3 $\{Rh(Cy_2P(CH_2)_3PCy_2)\}^+$/NBA: an η², η² σ-alkane complex. Addition of H_2 (1 bar, 298 K) to single-crystals of $[Rh(Cy_2P(CH_2)_3PCy_2)(NBD)][BAr^F_4]$, **[2-NBD][BAr$^F_4$]**, resulted in the rapid (~ 5 mins) formation of the σ-alkane complex $[Rh(Cy_2P(CH_2)_3PCy_2)(\eta^2\eta^2\text{-}NBA)][BAr^F_4]$, **[2-NBA][BAr$^F_4$]**, in a SC-SC transformation, as shown by single-crystal X-ray diffraction (Fig. 2) and $^{31}P\{^1H\}/^{13}C\{^1H\}$ SSNMR spectroscopies. The octahedral arrangement of $[BAr^F_4]^-$ anions is retained in **[2-NBA][BAr$^F_4$]**[39] while the central cation is a pseudo-square planar $\{RhL_2\}^+$ fragment bound with the alkane NBA through two *endo* Rh···H-C sigma interactions showing relatively short Rh···C distances [Rh···C 2.408(2)/2.402(2) Å] and rather acute ∠RhHC, e.g. Rh1-H1A-C1 105.1(2)º. These H-atoms were located and freely refined. These data suggest an η²,η² chelating Rh···H-C motif,[14,42] as corroborated by computational studies (see later). Despite the P-Rh-P bite-angle increasing compared with **[1-NBA][BAr$^F_4$]**[18] (e.g. Scheme 2B) the Rh···C distances are not different within error [cf. 2.389(3)/2.400(3) Å] and the structures are very similar, suggesting that the NBA ligand fits comfortably into the ligand pocket defined by the Cy-groups. This similarity is not strongly influenced by the anion microenvironment as evidenced by calculations on isolated cations (Section 2.7 and Supporting Materials). In the solid-state there are a number of weak C-H···F interactions between the NBA ligand and the $[BAr^F_4]^-$ anion, Figure S73.

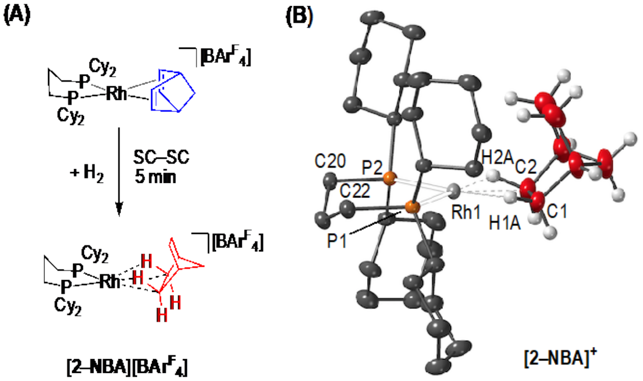

Figure 2. (A) Synthesis of **[2-NBA][BAr$^F_4$]**. (B) Cation of **[2-NBA][BAr$^F_4$]**. 50% displacement ellipsoids. Selected bond lengths (Å) and angles (º): Rh1···C1 2.408(2); Rh1···C2, 2.402(2); C1-C2, 1.554(3); Rh1-P1, 2.2065(4); Rh1-P2, 2.2049(4); P1-Rh1-P2 93.91(2)º, Rh1-H1A-C1, 105.1(2); Rh1-H2A-C2, 106.0(2); ∠P1P2Rh/Rh1C1C2, 5.15(7)º.

The $^{31}P\{^1H\}$ SSNMR spectrum of **[2-NBA][BAr$^F_4$]** shows two relatively sharp environments at δ = 50.6, 51.6 [*J*(RhP) ~ 170 Hz], while the $^{13}C\{^1H\}$ NMR spectrum is featureless between δ 110 and 50, demonstrating hydrogenation of the NBD. A $^1H/^{13}C$ Frequency Switched Lee-Goldburg (FSLG) HETCOR experiment at 298 K, which has been used to characterize E-H···M interactions in the solid-state (E = Si, C),[18,26,43] shows two strong correlations between δ(^{13}C) ~26 and δ(^1H) −2 which are consistent with the crystallographically inequivalent Rh···H-C interactions observed in the solid-state (Figure S13). An additional correlation [δ(^{13}C) 42/δ(^1H) −0.6][44] is assigned to the CH_2 bridge on the norbornane, which is affected by $[BAr^F_4]$ ring current effects as described for **[1-NBA][BAr$^F_4$]** and related complexes.[18,19,26]

Dissolving crystalline material of **[2-NBA][BAr$^F_4$]** in CD_2Cl_2 at 183 K results in free NBA being observed by ^1H NMR spectroscopy and a $^{31}P\{^1H\}$ NMR spectrum that is suggestive of a solvent-coordinated complex, $[Rh(Cy_2P(CH_2)_3PCy_2)(ClCH_2Cl)_n][BAr^F_4]$, δ 47.4 [*J*(RhP) = 198 Hz], similar to that reported for $[Rh(^iPr_2P(CH_2)_3P^iPr_2)(ClCH_2CH_2Cl)][BAr^F_4]$.[18] On warming, decomposition occurs via C-Cl activation to give a mixture of partially soluble chloride-bridged hydride dimers, e.g. $[Rh(Cy_2P(CH_2)_3PCy_2)H(\mu\text{-}Cl)]_2[BAr^F_4]_2$, that precipitate from solution and are best identified by ESI-MS. The formation of the $[BAr^F_4]^-$ coordinated zwitterion was not observed,[45] in contrast to **[1-NBA][BAr$^F_4$]** that forms **[1-BAr$^F_4$]** in CD_2Cl_2.[18] We suggest this is a consequence of the increased steric profile of the chelating phosphine $Cy_2P(CH_2)_3PCy_2$ versus $Cy_2P(CH_2)_2PCy_2$, disfavoring coordination of the, local to the metal center, planar and bulky $[BAr^F_4]^-$ anion, coupled with the wider bite-angle phosphines encouraging oxidative addition at Rh(I).[6]

2.4 $\{Rh(Cy_2P(CH_2)_3PCy_2)\}^+$/COA: A 12-electron Rh(I) complex supported by agostic interactions with an encapsulated non-bonding alkane.

Exposing single crystals of **[2-COD][BAr$^F_4$]** to H_2 for 3 hours results in, slower,[40,41] SC-SC hydrogenation and expulsion of cyclooctane (COA) from the metal-center to form formally

12–electron "naked"[46,47] $[Rh(Cy_2P(CH_2)_3PCy_2)]^+$, **[2]**$^+$. Remarkably the free alkane is retained inside the anion octahedral cavity to give $[Rh(Cy_2P(CH_2)_3PCy_2)][COA{\subset}BAr^F{}_4]$, **[2][COA⊂BAr$^F{}_4$]**, Scheme 3.

Scheme 3. Synthesis of [2][COA⊂BAr$^F{}_4$].

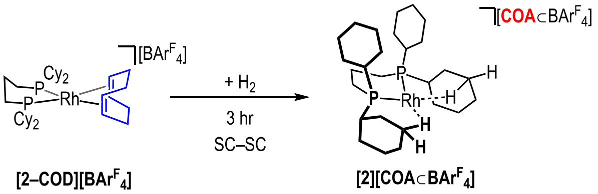

The solid–state structure of the cation **[2]**$^+$ (Fig. 3A) shows two γ–agostic[48-50] Rh···H–C interactions from the cyclohexyl rings [Rh···C3 2.91(1), Rh···C9 2.87(1) Å] that form in response to the unsaturation now at the Rh(I) metal center. The Rh1–P1–C1 angle reflects this, for example being more acute [108.9(3)º] than Rh1–P1–C13 [119.8(3)º]. The Rh–center also moves towards the C–H bonds involved in these agostic interactions, as shown by the angle between the planes ∠ P1P2C25C27/Rh1P1P2 = 42.6(2)º (Fig. 3B). The relatively long Rh···C distances, coupled with more open ∠RhHC angles, e.g. Rh1–H9A–C9 147.9(6)º, albeit the Hs–placed in calculated positions, suggests an η^1 Rh···H–C bonding motif for the agostic interactions, a view supported by calculations (see Section 2.7). This movement of the metal center keeps the phosphine ligand in essentially the same environment in the anion cavity, and maximizes the Rh···H–C agostic interactions, with two cyclohexyl group also enfolding the metal center.[51] It also retains the square planar geometry around Rh, with angles around the metal center = 360º. A minor, disordered, agostomeric[52] component is also present (~10%) in which the Rh–center swings up to interact with the chemically equivalent C15–H and C21–H bonds (Fig. 3C). The Rh–P distances in the major component [2.166(2) and 2.171(2) Å] are ~0.04 Å shorter than in **[2–NBA][BAr$^F{}_4$]**. Whether this reflects a weaker *trans*–influence of the *bis*–agostic Rh···H–C interactions in **[2][COA⊂BAr$^F{}_4$]** compared with the intermolecular interactions in **[2–NBA][BAr$^F{}_4$]**, or is a consequence of the metal's unusual disposition, is not clear. Although formally 2–coordinate group 9 complexes are known,[53,54] albeit rare, as far as we are aware the cation in **[2][COA⊂BAr$^F{}_4$]** is the first example reported with a chelating phosphine.

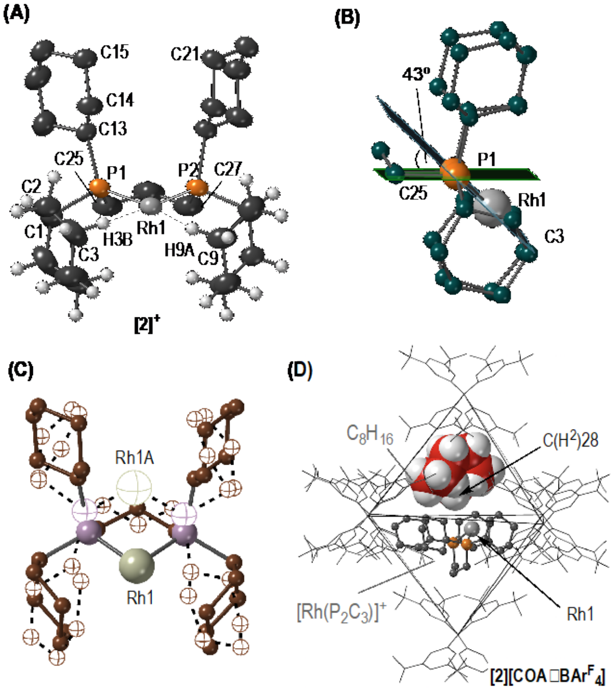

Figure 3. **(A)** Cation of **[2][COA⊂BAr$^F{}_4$]**. 50% displacement ellipsoids, only the major disordered component shown. Selected bond lengths (Å) and angles (º): Rh1···C3 2.912(10); Rh1···C9, 2.873(10); Rh1–P1, 2.171(2); Rh1–P2, 2.166(2); P1–Rh1–P2 91.21(8)º; ∠P1P2C25C27/Rh1P1P2 = 42.6(2)º. **(B)** Displacement of the Rh–center in **[2]**$^+$ towards the agostic C–H bonds in the major disordered component. **(C)** Ball-and-stick representation of the two disordered components in **[2]**$^+$. **(D)** Packing diagram of **[2][COA⊂BAr$^F{}_4$]** showing O_h arrangement of $[BAr^F{}_4]^-$, COA (C = red) shown at van der Waals radii and only one disordered component shown; Rh1···C28, 3.74(1) Å.

The expelled alkane, COA, sits encapsulated[55,56] within the anion–framework (Fig. 3D), essentially equally disordered between two boat–chair conformations.[57] The closest Rh···C distance is 3.74(1) Å (C28), approaching the Rh–center above the square plane, suggesting no significant, and at best very weak, interaction with the metal center. This distance is similar to that measured in $[U(ArO)_3tacn(c\text{-}C_6H_{11}Me)]$ [3.864(7) Å, albeit U *versus* Rh] where a bonding interaction was suggested,[58] although studies on related uranium complexes suggest such as distance reflects a non–bonding interaction.[59]

In the 158 K $^{31}P\{^1H\}$ SSNMR spectrum of **[2][COA⊂BAr$^F{}_4$]** only two broad (fwhm ~ 400 Hz) environments are observed at δ 51.3 and δ 48.1 in an approximate 1:1 ratio. Coupling to ^{103}Rh was not resolved. These do not vary significantly in chemical shift or relative intensity at 298 K. The observation of only 2 signals suggests that the disorder observed in the cation could be static (with coincident signals) or dynamic[60] (and fast[61]) on the NMR timescale, but that no change is observed on changing the temperature suggests the former. $^{13}C\{^1H\}$ SSNMR spectrum shows a featureless region between δ 115 and 43, indicating that the COD has been hydrogenated to COA, which is observed as a sharp signal at δ 25.7. This assignment is supported by a Non-Quaternary Suppression experiment (NQS) which, as well as detecting quaternary carbons, identifies CH$_n$ groups that experience motion in a frequency range similar to, or greater than the ^{1}H–^{13}C dipolar coupling.[62,63] In the 158 K NQS spectrum a single prominent signal remains at δ 25.7 in the alkyl region, compared with the ^{13}C{^{1}H} SSNMR spectrum (Figure 4A). This peak remains at 298 K.[39] These data are consistent with the encapsulated COA undergoing a low energy site–exchange within the cavity (Figure 4B), suggested to be a combination of 1,2–jumps and/or exchange between the two disordered COA components.[64] To calibrate our observations, a variable temperature NQS experiment on **[1–NBA][BAr$^F_4$]** showed a NBA fragment undergoing motion at 298 K which is halted at 158 K – fully consistent with previous variable temperature–SSNMR studies (Figure S3).[26] **[2][COA⊂BAr$^F_4$]** is not stable in solution. Vacuum transfer of CD$_2$Cl$_2$ onto solid **[2][COA⊂BAr$^F_4$]** and warming to 183 K resulted in a precipitate that was persistent on warming to room temperatures. ESI–MS shows this to contain multiple dimeric hydrido–chlorides.

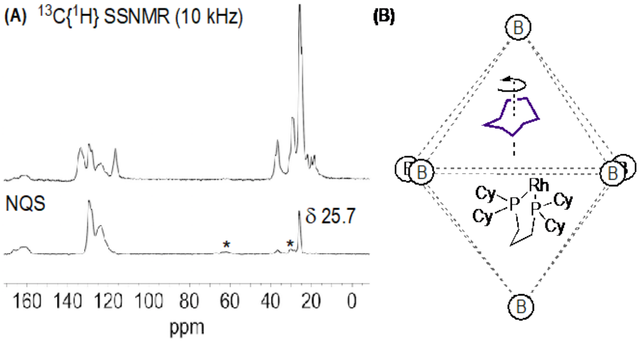

Figure 4. (A) ^{13}C{^{1}H} SSNMR spectra (10 kHz, 158 K) and NQS spectra of **[2][COA⊂BAr$^F_4$]** (10 kHz, 158 K). * = spinning–side band. **(B)** Proposed fluxional processes (Ⓑ = [BAr$^F_4$])

The structural changes evident between **[2–NBA][BAr$^F_4$]** – a η^{2}η^2 σ–alkane complex – and **[2][COA⊂BAr$^F_4$]** – with a non–bonding alkane – can be traced back to the change in hydrocarbon, as the {ML$_2$}$^+$ fragment is the same. Consideration of the van der Waals surfaces of NBA versus COA, Figure 5, shows that the latter presents a larger steric profile to the metal center. We suggest that this, alongside possible conformational preferences for metal binding of the alkane and non–covalent F···H–C interactions in the microenvironment (see Figure S73 and S76), are drivers for the different structural motifs observed.

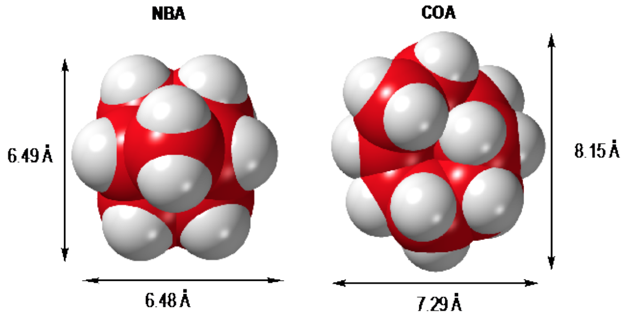

Figure 5. van der Waals[65] surfaces for NBA and COA.

2.5 {Rh(Cy$_2$P(CH$_2$)$_4$PCy$_2$)}$^+$/NBA: A η^2,η^2–σ–alkane complex.

Addition of H$_2$ to single–crystals of [Rh(Cy$_2$P(CH$_2$)$_4$PCy$_2$)(NBD)][BAr$^F_4$], **[3–NBD][BAr$^F_4$]**, resulted in a fast (~5 mins as measured by ^{31}P{^{1}H} SSNMR spectroscopy) SC–SC transformation to give the corresponding σ–alkane complex [Rh(Cy$_2$P(CH$_2$)$_4$PCy$_2$)(η^{2}η^2–NBA)][BAr$^F_4$], **[3–NBA][BAr$^F_4$]**, Figure 6. The solid–state structure of **[3–NBA][BAr$^F_4$]** reveals a σ–bound NBA ligand, with two Rh···H–C interactions using the *endo* C–H bonds (H–atoms located). Despite the bite–angle increasing further compared with **[1–NBA][BAr$^F_4$]** and **[2–NBA][BAr$^F_4$]** the key–metrics associated with this interaction remain essentially unchanged: Rh1–C1 2.399(2) Å, Rh1–C2 2.396(2) Å. ^{31}P{^{1}H}, ^{13}C{^{1}H} SSNMR and ^{1}H/^{13}C FLSG HETCOR data (Figure S33–S36) are fully consistent with the solid–state structure, i.e. ^{31}P{^{1}H} δ 66.7 [*J*(RhP) = 201 Hz], 49.4 [*J*(RhP) = 196 Hz]. Dissolution of **[3–NBA][BAr$^F_4$]** in CD$_2$Cl$_2$ resulted in a yellow precipitate, identified by ESI–MS, again, as a mixture of dimeric hydrido/chlorides.

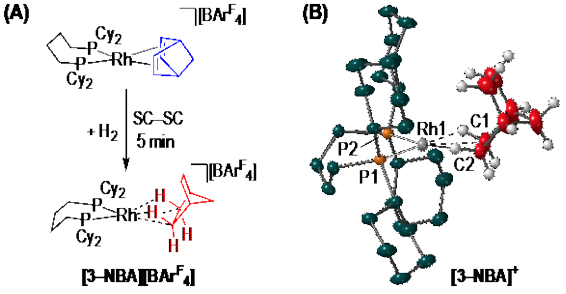

Figure 6. (A) SMOM synthesis of **[3–NBA][BAr$^F_4$]**. **(B)** Cation of **[3–NBA][BAr$^F_4$]** (50% displacement ellipsoids): Rh1···C1 2.399(2); Rh1···C2, 2.396(2) Å; Rh1–P1, 2.2154(4); Rh1–P2, 2.2215(4); P1–Rh1–P2 97.87(2)º.

Increasing the bite angle of the phosphine promoted different *reactivity* in the resulting σ–alkane complex. Surprisingly given that the structural metrics have not changed significantly from the smaller bite–angle congeners, **[3–NBA][BAr$^F_4$]** is not stable when exposed to a moderate vacuum for 3 days. Crystallinity is lost and SSNMR spectroscopy shows the formation of multiple species – as yet unidentified. Thus, although the binding of the NBA ligand appears to not be influenced significantly by the increase in bite angle of the chelating phosphine, in the measured ground–state structure steric pressure and/or enhanced stability of any decomposition products as driven by the change in phosphine appear to promote reactivity towards loss of NBA. Hydrogenation of single–crystals of **[3–COD][BAr$^F_4$]** in a solid/gas reaction resulted in loss of crystallinity.[39] We have not characterized the product of this further.

2.6 {Rh(Cy$_2$P(CH$_2$)$_5$PCy$_2$)}$^+$/COA and NBA: Phosphine ligand backbone C–H activation, structural reorganization with retention of crystallinity and Rh(III) η^1-σ–alkane complexes.

Addition of H$_2$ to crystalline **[4–NBD][BAr$^F_4$]** resulted in a rapid (~5 minutes as measured by ^{31}P{^{1}H} SSNMR spectroscopy) SC–SC reaction. Analysis of the product formed using single–crystal X–ray diffraction was hampered by long range disorder, which is also present in the starting material. The structure was modelled using a supercell (Z’ = 2) which gave a satisfactory solution (*R* = 15.7%) that allowed for the gross structure of the cation to be determined, Figure 7, but does not allow for detailed metrics to be discussed. Hydrogen atoms were not located, and the NBA fragments formed by hydrogenation were necessarily modelled as rigid bodies. There are two chemically very similar, but crystallographically independent, cations in this supercell in which each has a disordered NBA over two conformations (Figure 7C). There is no crystallographically imposed local symmetry. The O_h arrangement of anions in relation to each cation is retained (Figure S83–S88).

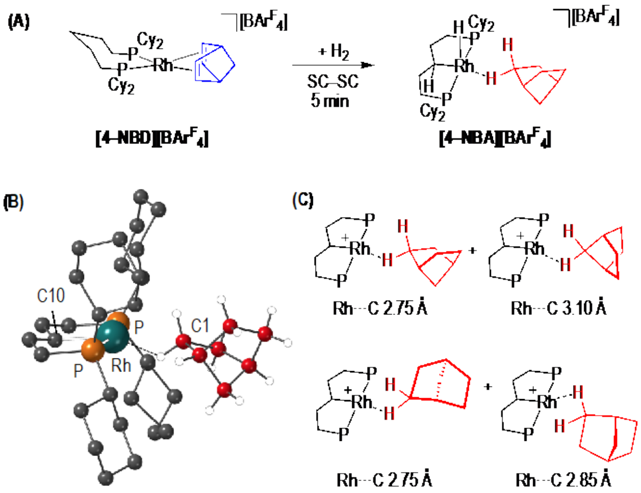

Figure 7. (**A**) Synthesis of [**4–NBA**][**BAr$^{F}_{4}$**]; (**B**) Ball and stick representation of the one of the crystallographically–independent cations in the solid–state showing one disordered NBA component, Rh–C10, ~2.04 Å; P–Rh–P, ~167º; (**C**) Representation of the four disordered NBA fragments at the two crystallographically–independent cations with Rh···C(alkane) distances. Hydride positions were not determined, Cy–groups not shown.

Despite the challenges associated with structural identification, immediately apparent is that the phosphine pentamethylene backbone has undergone a C–H activation in the solid–state to form a wide bite angle *trans*–spanning phosphine PCP pincer complex. Such intramolecular C–H activation with a $R_2P(CH_2)_5PR_2$ ligand has precedent in solution studies, either to form a hydrido–alkyl complex[66-68] or through a further α–elimination to give a diphosphino-carbene complex.[69] Solution trapping experiments (*vide infra*) show that the former has occurred in [**4–NBA**]$^+$, and thus a formulation of [Rh($Cy_2P(CH_2)_2(CH)(CH_2)_2PCy_2$)H(η–NBA)][BAr$^{F}_{4}$], [**4–NBA**][**BAr$^{F}_{4}$**] is proposed. The disordered NBA ligand shows a range of Rh···C distances to the Rh(III) center [2.75 – 3.10 Å] and interacts via either the basal or bridge methylene groups. These distances reflect weak (at best) σ–interactions compared to, e.g., [**2–NBA**][**BAr$^{F}_{4}$**];[49] while this spread suggests that the NBA fragment finds a better spatial fit with the {RhPCP}$^+$ fragment for some conformations over others. The data, clearly, do not allow the precise binding mode of the alkane (η^1–HC, η^3–H_2C[70]) to be determined. A related SC–SC N–C oxidative addition at a Rh(I) center has been reported in Rh–PNP pincer complexes.[71] [**4–NBA**][**BAr$^{F}_{4}$**] is stable indefinitely in a Ar-filled glovebox or under vacuum.

The 298 K ^{13}C{^{1}H} SSNMR spectrum of [**4–NBA**][**BAr$^{F}_{4}$**] shows a featureless region between δ 116 and 59, demonstrating hydrogenation of the diene. The 298 K ^{31}P{^{1}H} SSNMR shows a tightly–coupled ABX system,[72] which is less well resolved at 158 K, consistent with inequivalent *trans*–phosphines that are in chemically very similar environments bound to a Rh(III) center: δ 64.1, 63.4 [*J*(RhP) ~ 105, *J*(PP) 325 Hz] (Figure S49–S50). The ^{13}C NQS spectrum at 158 K shows at least four signals grouped between δ 38–35 and δ 29–27, in the region associated with aliphatic C–H groups, that indicate a low–energy molecular motion of the NBA ligand within the cavity of the cage (Figure S54). Such a low energy process is consistent with the disorder of the NBA fragment modelled in the solid–state. In the 158 K FSLG HETCOR spectrum cross peaks between these aliphatic signals in the ^{13}C SSNMR spectrum and low–field peaks in the ^{1}H projection (δ –1.8 to –2.6) are observed. We assign these to the Rh···H–C interactions, although we cannot discount ring–current effects from the proximal Ar^{F} groups causing such a high–field shift in other C–H bonds.[18,26]

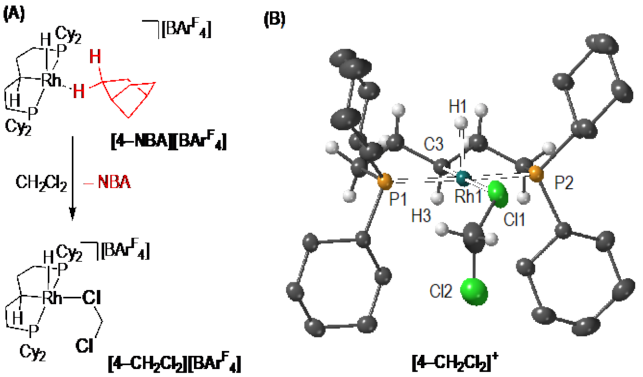

Figure 8. (**A**) Synthesis of [**4–CH_2Cl_2**][**BAr$^{F}_{4}$**]; (**B**) Cation of [**4–CH_2Cl_2**][**BAr$^{F}_{4}$**] (50% displacement ellipsoids): Rh1–C3, 2.074(2) Å; Rh1–P1, 2.3182(5); Rh1–P2, 2.3099(5); Rh1–Cl1, 2.6032(5); Rh1–H1, 1.65(4); P1–Rh1–P2 167.04(2)º.

Unlike for [**2–NBA**][**BAr$^{F}_{4}$**] or [**3–NBA**][**BAr$^{F}_{4}$**], dissolving [**4–NBA**][**BAr$^{F}_{4}$**] in CD_2Cl_2 gave a stable complex that could be characterized by solution NMR spectroscopy and single–crystal X-ray diffraction (crystals grown from CH_2Cl_2/pentane) as [Rh($Cy_2P(CH_2)_2(CH)(CH_2)_2PCy_2$)H($\kappa^1$–$ClCH_2Cl$)][BAr$^{F}_{4}$], [**4–$CH_2Cl_2$**][**BAr$^{F}_{4}$**], Figure 8, in which the NBA ligand has been replaced by a CH_2Cl_2 ligand. Vacuum transfer of the volatiles demonstrates NBA is liberated, consistent with the initial solid/gas hydrogenation of the NBD to form [**4–NBA**][**BAr$^{F}_{4}$**]. The molecular structure of [**4–CH_2Cl_2**][**BAr$^{F}_{4}$**], Figure 8B, does not suffer from disorder and clearly shows the *trans*–spanning PCP–pincer motif suggested for [**4–NBA**][**BAr$^{F}_{4}$**]. The Rh–hydride (H1) was located, sitting *trans* to a vacant site, and *anti* to the remaining hydrogen associated with the C–H activated methylene group (H3). This stereochemistry is as expected for an intramolecular C–H activation.[66,68] A CH_2Cl_2 molecule has displaced the labile NBA fragment. Displacement of a weakly bound σ–alkane ligand by halogenated solvent is well–established,[18,28,30] and the structure is consistent with other crystallographically characterized Rh–$ClCH_2Cl$ complexes.[49,73,74] [**4–CH_2Cl_2**][**BAr$^{F}_{4}$**] is a 16–electron Rh(III) complex, but there is no evidence for any significant supporting agostic interaction from the cyclohexyl groups: closest Rh···C = 3.261(3) Å. Although this is not a SC–SC transformation, the O_h arrangement of anions is retained in the extended solid–state structure of recrystallized matrial.

Solution NMR data for **[4–CH$_2$Cl$_2$][BAr^F$_4$]** at 298 K (CD$_2$Cl$_2$) reveal a fluxional process is occurring. In the ^{1}H NMR spectrum relatively broad signals are observed for the phosphine ligand, and no characteristic signal due to the C–H activated methylene (ca. 3 ppm[68]) or Rh–H were observed. The ^{31}P{^{1}H} NMR spectrum showed a relatively sharp doublet at δ 66 [*J*(RhP) 121 Hz]. Cooling to 243 K results in a sharpening of the aliphatic region in the ^{1}H NMR spectrum, and two new signals at δ 2.71 and –27.2 [d, *J*(RhH) = 55 Hz, br, fwhm ~ 40 Hz] appear which integrate to 1 H each. These are assigned to the C–H activated methylene (i.e. C3) and Rh–H respectively, the latter with a chemical shift that places it *trans* to a vacant site.[66,75,76] A spin–saturation experiment at this temperature shows that these two signals are undergoing slow mutual exchange. The ^{31}P{^{1}H} NMR spectrum is still a doublet but shifted slightly to lower field [δ 64.4]. These low temperature data are fully consistent with the solid–state structure of **[4–CH$_2$Cl$_2$][BAr^F$_4$]**. An exchange process that involves reversible reductive C–H bond forming/C–H oxidative addition is proposed – as suggested for closely related systems[66] – and DFT calculations confirm this is favoured ($\Delta G^{\ddagger}_{calc}$ = 18.7 kcal/mol) over an alternative α–elimination process via a diphosphino-carbene intermediate ($\Delta G^{\ddagger}_{calc}$ = 27.4 kcal/mol, see Figure S105, Supporting Materials).[69] It is also likely that the bound CH$_2$Cl$_2$ molecule is undergoing rapid exchange at the metal center with the solvent.[77]

Scheme 4. Synthesis of [4–COA][BAr^F$_4$]

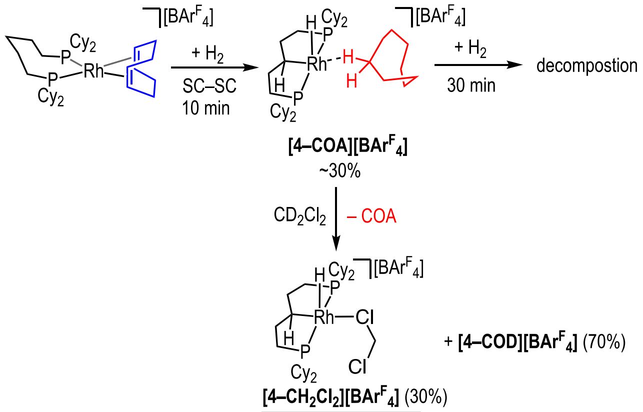

If **[4–COD][BAr^F$_4$]** is subjected to H$_2$ in the solid–state, after 30 mins crystallinity is lost. However, if the reaction is stopped after only 10 minutes and the resulting single crystals quickly transferred to an X-ray diffractometer and cooled to 150 K, the resulting analysis shows that a new complex is formed in 30% yield in a SC–SC process, with the remainder being unreacted **[4–COD][BAr^F$_4$]**. These data showed this new complex to be **[4–COA][BAr^F$_4$]**, [Rh(Cy$_2$P(CH$_2$)$_2$(CH)(CH$_2$)$_2$PCy$_2$)H(η^1-COA)][BAr^F$_4$]. Although the single–crystal refinement showed a mixture of **[4–COD][BAr^F$_4$]** (70%) and **[4–COA][BAr^F$_4$]** (30%) in the O_h–anionic cage, refinement of the constituent components gave a reliable and robust solution (*R* = 9.6%).

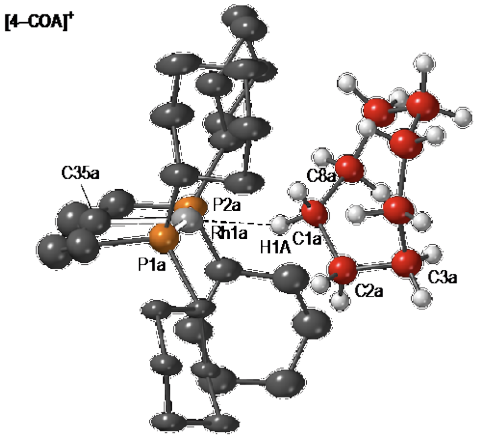

Figure 9. Cation of [4–COA][BAr^F$_4$] (30% displacement ellipsoids), H atoms not located, disordered **[4–COD][BAr^F$_4$]** not shown: Rh1a···C1a, 2.90(3) Å; Rh1–C35a 2.08(3) Å, C1a–C2a, 1.477(2) Å; C1a–C8a, 1.45(2); P1a–Rh1a–P2a 168.5(3)º; C35a–Rh1a···C1a, 174.6(9); Rh1a–H1A–C1a 140.7(2).

The molecular cation of **[4–COA]$^+$** is shown in Figure 9. This shows a C–H activated, *trans*–spanning, diphosphine "PCP" pincer ligand with a cyclooctane located in close proximity to the Rh(III) metal center [Rh1a···C1a 2.90(3) Å]. The COA ligand is not disordered and shows that all the C–C bonds are single [1.46(2) – 1.48(2) Å]. The Rh···C distance is very long compared with other Rh···H–C σ–alkane complexes, cf **[1–pentane][BAr^F$_4$]**, 2.522(5)Å in which the pentane acts as a bidentate ligand.[78] However, it is considerably shorter than found in **[2][COA⊂BAr^F$_4$]** (where we propose a minimal interaction at best), and is of a similar distance to the weak agostic interaction in *trans*-[Rh(2,2'-biphenyl)(P^{i}Bu$_3$)$_2$][BAr^F$_4$] [2.979(4) Å], as also interrogated by QTAIM analysis.[49] This distance, combined with a rather open Rh1a–H1A–C1a (albeit the H-placed in a calculated position) of 140.7(2)º, points to a η^1 Rh···H–C interaction. The hydrogen atoms were not located in **[4–COA]$^+$**, but as dissolution of the crystalline material in CD$_2$Cl$_2$ formed **[4–CD$_2$Cl$_2$][BAr^F$_4$]**/free COA alongside **[4–COD][BAr^F$_4$]** in a 30:70 ratio, Scheme 4, the same Rh–H, C–H activated motif as for **[4–NBA][BAr^F$_4$]** is proposed. As for the other σ–alkane structures reported here, there are multiple stabilizing C–H···F interactions between the alkane and proximal CF$_3$ groups in the lattice (Figure S91).

Complex **[4–COA][BAr^F$_4$]** is a σ–alkane complex in which only one Rh···H–C interaction is present, being related to structures characterized using solution and DFT techniques, such as [Re(η^6–C$_6$Me$_6$)(CO)$_2$(C$_5$H$_{10}$)][Al(OR^f)$_4$][31] or Rh(η^5–C$_5$H$_5$)(CO)(C$_8$H$_{16}$)][79] respectively. However, as far as we are aware this is the first structurally determined example of an alkane interacting η^1– with a transition metal center. Such motifs have been probed in the ps-timescale using fast time-resolved infrared spectroscopy (TRIR) combined with DFT calculations, and are early intermediates in the oxidative addition of alkanes to coordinatively unsaturated metal centers.[80-82] Valence isoelectronic amine–borane and silane complexes with η^1–M···H–E coordination have been reported and show comparable structural metrics to **[4–COA][BAr^F$_4$]**, such as wide M–H–E angles and long M···E distances: [Ir(POCOP)H(η^1-HSiEt$_3$)][B(C$_6$F$_5$)$_4$], **A**, [83] (POCOP = 2,6-[OP^{t}Bu$_2$]$_2$C$_6$H$_3$) and [Rh(κ^3-Xantphos)(H)$_2$(η^1-H$_3$B·NMe$_3$)][BAr^F$_4$], **B**, [84] Chart 1. Of course the increased polarity of the E–H bond in these analogs will make a significant contribution to bonding and thus they are sufficiently stable to observed using solution NMR techniques, unlike **[4–COA][BAr$^{F}_{4}$]**.

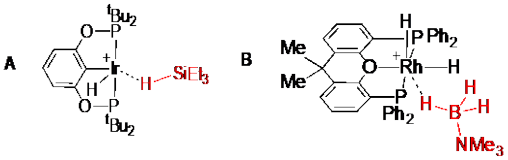

Chart 1. Examples of η^1–coordinated σ–complexes. Anions are not shown.

If hydrogenation of **[4–COD][BAr$^{F}_{4}$]** is continued for a total of 30 minutes decomposition to an, as yet unidentified, product(s) is observed upon dissolving in CD_2Cl_2, from which a featureless ^{31}P{^{1}H} NMR spectrum and a very broad ^{1}H NMR spectrum are observed. We speculate that this signals the formation of a paramagnetic Rh(II) dimeric complex on dissolution,[85] but the identity of this species remains to be resolved. Attempts to obtain meaningful SSNMR data for **[4–COA][BAr$^{F}_{4}$]** were hampered by temporal and temperature sensitivity that was amplified by the requirement to use finely crushed material for analysis by SSNMR that meant that crystallinity is lost much faster than for larger samples. In the ^{31}P{^{1}H} SSNMR spectrum at 158 K a major, broad, peak at δ 64 is observed (being similar to that seen for **[4–NBA][BAr$^{F}_{4}$]**), alongside **[4-COD][BAr$^{F}_{4}$]** and decomposition products. The sensitivity of **[4–COA][BAr$^{F}_{4}$]** contrasts with the relative stability of **[4–NBA][BAr$^{F}_{4}$]** or **[2][COA⊂BAr$^{F}_{4}$]** and perhaps reflects the combination of the different steric profile of the alkane in the former (NBA versus COA) combined with the stabilizing influence of agostic interactions in the latter.

[4–NBA][BAr$^{F}_{4}$] and **[4–COA][BAr$^{F}_{4}$]** are shown to have very similar structures, with the former's stability allowing for a more detailed characterization by SSNMR spectroscopy and the latter providing a good structural solution by X-ray crystallography. Combined they thus provide a convincing analysis as a weakly bound σ–alkane complex bound η^1– at a Rh(III) center. We believe they are the first Rh(III) σ–alkane complexes isolated, or observed, by any method.

2.7 Computational Studies

Periodic DFT calculations were performed on the extended solid state structures of **[X-NBA][BAr$^{F}_{4}$]** (X = 1,[86] 2 and 3), **[2][COA⊂BAr$^{F}_{4}$]** and **[4-COD][BAr$^{F}_{4}$]** to assess the structure and bonding of these species (see Supporting Materials for details and tables of computed structures). For the **[X-NBA][BAr$^{F}_{4}$]** series geometries optimised with the PBE-D3 approach provided good agreement with the experimental structures. For **[2][COA⊂BAr$^{F}_{4}$]** both the major and minor components were computed and structural metrics around the Rh centres were again well reproduced. However, more movement of the COA was seen in these calculations, perhaps reflecting the absence of significant bonded interactions between Rh and the COA (see below). For **[4–COA][BAr$^{F}_{4}$]** the calculations slightly underestimate the Rh1···C1 distance (calc: 2.80 Å; exp: 2.90(3) Å). Given the variations between computed and experimental structures across the range of systems under consideration, the subsequent analyses were based on computed structures in which the Rh, C, B and P positions were taken from the crystallographic studies and the H and F atoms were optimised with the PBE-D3 approach. Selected distances involving key H atom positions optimized on this basis are shown in Figure 10. A more quantitative analysis of bonding was then provided by Quantum Theory of Atoms in Molecules (QTAIM) and Natural Bond Orbital (NBO) 2nd order perturbation donor-acceptor interaction analyses performed on the isolated cations shown in Figure 10, while non-covalent interaction (NCI) plots were run on ion-pairs featuring the nearest-neighbour [BAr$^{F}_{4}$]$^-$ anion.

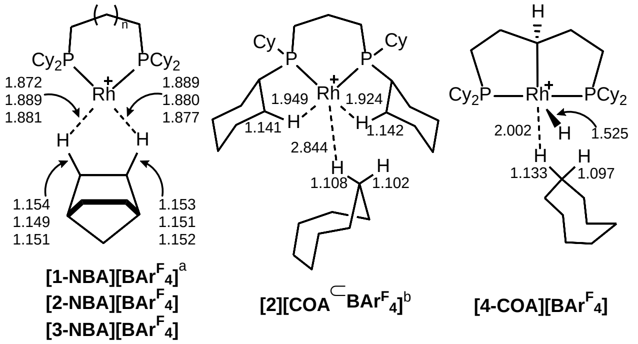

Figure 10. Computed distances (Å) involving key H atoms in **[X-NBA][BAr$^{F}_{4}$]** (X = 1, 2 and 3; n = 0, 1 and 2 respectively), **[2][COA⊂BAr$^{F}_{4}$]** and **[4-COD][BAr$^{F}_{4}$]**. ^{a}*endo*-C–H bonds indicated: all *exo*-C–H bond distances fall between 1.094 and 1.100 Å ^{b}Based on optimization of the major component.

2.7.1 [X-NBA][BAr$^{F}_{4}$] (X = 1, 2 and 3). Computed structures for all three species show short Rh···H11/H21 contacts of around 1.88 Å and elongation of the C1-H11/C2-H21 bonds to *ca.* 1.15 Å consistent with the presence of two 3c-2e C–H···Rh σ-interactions in each case. QTAIM and NBO analyses on the **[2-NBA]$^+$** cation confirm this (Figure 11A-C), with the presence of Rh–H11 and Rh–H21 bond paths and reduced bond critical point (BCP) metrics for C1–H11 and C2–H21 compared to the spectator C1–H21/C2–H22 bonds. NBO calculations highlight the dominance of C–H→Rh σ-donation into the *trans*-σ*$_{Rh-P}$ orbital, reinforced by π-back-donation from a Rh lone pair (d orbital) and the *cis*-σ$_{Rh-P}$ bonding orbital. Similar results were computed for **[1-NBA]$^+$** and **[3-NBA]$^+$** (see Supporting Materials) indicating that changing the bite angle has a minimal effect on the Rh–NBA interaction.

Figure 11D shows the NCI plot of the **[2-NBA][BAr$^{F}_{4}$]** ion-pair and reveals a broad curved feature running roughly parallel to the H11–C1–C2–H21 bonds. This reflects the chelating nature of the NBA ligand and is predominantly stabilising (blue) in character, while also exhibiting a central destabilising (orange/red) region that is consistent with the presence of the ring critical point (RCP) in the QTAIM study. Some destabilising character is also seen between Rh and the center of the two C–H bonds (see detail in Figure 11E). This suggests two cyclic {RhCH} features in the electron density topology that are consistent with an η^2-interaction and the significant contribution of classical Rh(dπ) to σ*$_{C-H}$ π-back donation identified in the NBO analysis. This also highlights how the NCI approach can amplify the insight gained from the local QTAIM critical points.[87-89] These features contrast with the more localised η^1-interactions associated with C–H···Rh bonding in **[2][COA⊂BAr$^{F}_{4}$]** and **[4-COA][BAr$^{F}_{4}$]** (see below). The NCI plot also highlights broad swathes of green that indicate weak, dispersive stabilization between the NBA ligand and (i) the aryl groups of the borate anions and (ii) the cyclohexyl substituents of the cation. Thus intermolecular dispersion interactions play a crucial role in stabilizing these alkane ligands within the binding 'pocket'.[90] Similar NCI plots were obtained for **[1-NBA][BAr$^F_4$]** and **[3-NBA][BAr$^F_4$]** and a side-by-side comparison is provided in Figure S100 in the Supporting Materials.

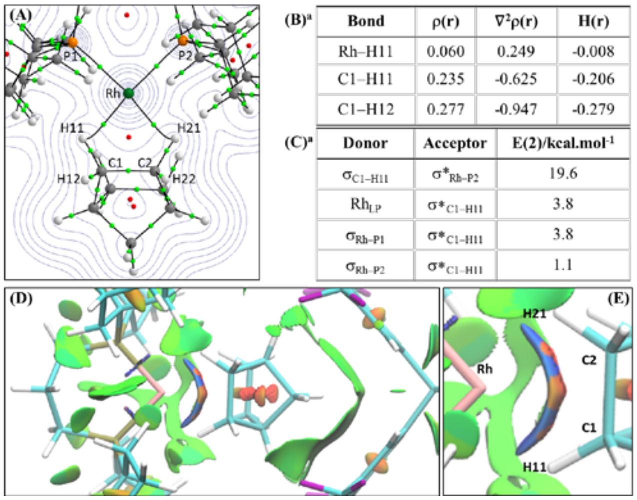

(B)[a]

Bond	ρ(r)	$\nabla^2\rho(r)$	H(r)
Rh–H11	0.060	0.249	-0.008
C1–H11	0.235	-0.625	-0.206
C1–H12	0.277	-0.947	-0.279

(C)[a]

Donor	Acceptor	E(2)/kcal.mol^{-1}
σ_{C1-H11}	σ^*_{Rh-P2}	19.6
Rh_{LP}	σ^*_{C1-H11}	3.8
σ_{Rh-P1}	σ^*_{C1-H11}	3.8
σ_{Rh-P2}	σ^*_{C1-H11}	1.1

Figure 11. **(A)** Molecular graph of the **[2-NBA]**$^+$ cation; density contours plotted in the RhH11H21 plane with BCPs (green) and RCPs (red); **(B)** Key BCP metrics, and **(C)** donor-acceptor interactions associated with the Rh–H11C1 interaction; (**D**) NCI plot of the **[2-NBA][BAr$^F_4$]** ion-pair; isosurface generated for s = 0.3 au and -0.07 < ρ < 0.07 au); **(E)** detail of the {Rh-NBA} interaction. [a]similar data are obtained for the Rh–H21, C2–H21 and C2–H22 interactions.

2.7.2. [2][COA⊂BAr$^F_4$]. QTAIM and NBO data for the **[2]**$^+$ cation are displayed in Figure 12A-C. Rh–H3B and Rh–H9A bond paths signal the presence of intramolecular agostic interactions. The associated Rh···H contacts are longer (ca. 1.94 Å), and the corresponding C–H distances shorter (ca. 1.14 Å), than in the **[X-NBA]**$^+$ series, suggesting weaker interactions in **[2]**$^+$. This is confirmed by reduced ρ(r) values at the Rh–H BCPs and lower $\sigma_{C\text{-}H}$ to *trans*-σ^*_{Rh-P} σ-donation via NBO. NBO, however, also suggests a similar degree of back donation as **[2-NBA]**$^+$, although this is not classical Rh(dπ) to σ^*_{C-H} π-back donation but rather involves contributions from both the *cis*- and *trans*-σ_{Rh-P} bonds (see also the discussion of **[4-COA]**$^+$ below). This suggests an η^1-C-H→Rh interaction and is supported by the NCI plot which highlights these stabilising agostic interactions with well-defined, localized blue disks (Figures 12D and E).

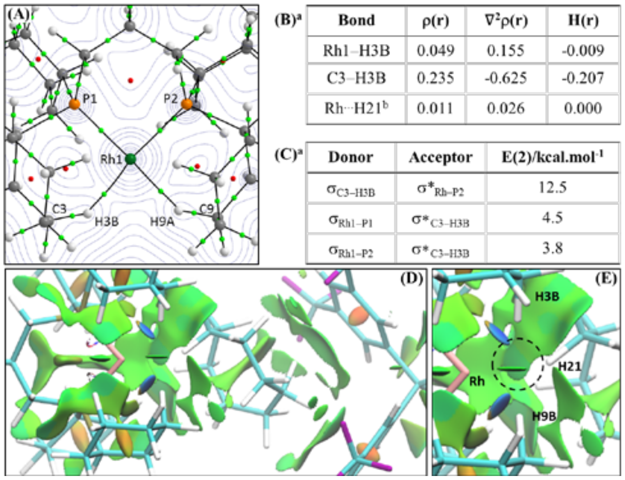

(B)[a]

Bond	ρ(r)	$\nabla^2\rho(r)$	H(r)
Rh1–H3B	0.049	0.155	-0.009
C3–H3B	0.235	-0.625	-0.207
Rh···H21[b]	0.011	0.026	0.000

(C)[a]

Donor	Acceptor	E(2)/kcal.mol^{-1}
σ_{C3-H3B}	σ^*_{Rh-P2}	12.5
σ_{Rh1-P1}	σ^*_{C3-H3B}	4.5
σ_{Rh1-P2}	σ^*_{C3-H3B}	3.8

Figure 12. **(A)** Molecular graph of the **[2]**$^+$ cation; density contours plotted in the RhH3AH9A plane with BCPs (green) and RCPs (red); **(B)** Key BCP metrics and **(C)** donor-acceptor interactions associated with the Rh–H11C1 interaction; **(D)** NCI plot of the **[2][COA⊂BAr$^F_4$]** ion-pair; isosurface generated for s = 0.3 au and -0.07 < ρ < 0.07 au; **(E)** Detail highlighting the region around Rh (the disk within the circled region arises from an interaction between cyclohexyl hydrogens and sits well above the coordination plane). [a] similar data are obtained for the Rh–H9A and C9–H9A interactions. [b] COA omitted from the molecular graph for clarity, see Supporting Materials.

The closest Rh···COA contact in **[2][COA⊂BAr$^F_4$]** is via H21 with a computed distance of 2.844 Å. This is well within the sum of the van der Waals radii of Rh and H (3.64 Å)[65] and a weak BCP is computed between these centers (ρ(r) = 0.011eÅ^{-3}).[91] No equivalent donor-acceptor interaction is computed with NBO, although the NCI plot does suggest a weak, stabilizing feature between Rh and H21 (see Figures 13D and E). This is part of a broad area of weakly stabilizing interactions between the COA and the [2]$^+$ cation, suggesting any direct covalent Rh···H21 interaction is at best very weak, if it exists at all. The COA is further stabilized within the cavity by dispersive interactions with the two proximate aryl substituents of the [BAr$^F_4$]$^-$ anion.[92]

2.7.3. [4-COA][BAr$^F_4$]. The computed structure of **[4-COA][BAr$^F_4$]** shows a Rh–H11 distance of 2.002 Å and an elongated C1–H11 distance of 1.13 Å (Figure 10). These, along with the computed Rh···H11 BCP metrics (Figure 13) suggest a somewhat weaker σ-interaction than in the **[2]**$^+$ cation, although NBO indicates a similar degree of σ-donation and, if anything, greater back donation in this case. A blue/green disk in the NCI plot confirms this η^1 C1–H11→Rh σ-interaction, as well as highlighting broad areas of stabilising dispersion interactions with the cyclohexyl substituents and the [BAr$^F_4$]$^-$ aryl groups.

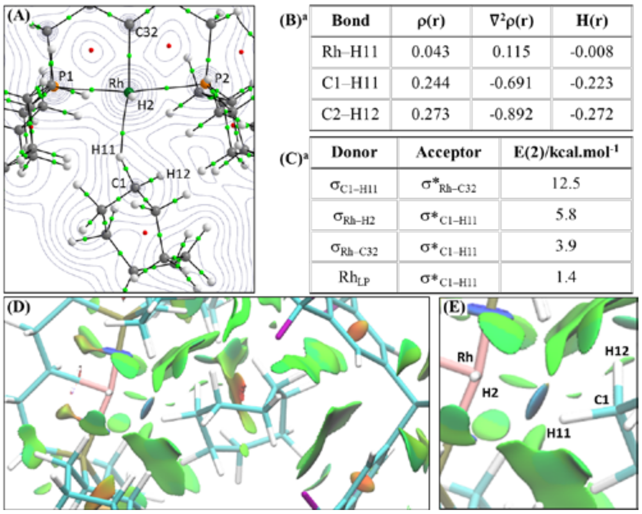

Bond	ρ(r)	$\nabla^2\rho(r)$	H(r)
Rh–H11	0.043	0.115	-0.008
C1–H11	0.244	-0.691	-0.223
C2–H12	0.273	-0.892	-0.272

Donor	Acceptor	E(2)/kcal.mol^{-1}
σ_{C1-H11}	σ^*_{Rh-C32}	12.5
σ_{Rh-H2}	σ^*_{C1-H11}	5.8
σ_{Rh-C32}	σ^*_{C1-H11}	3.9
Rh_{LP}	σ^*_{C1-H11}	1.4

Figure 13. (**A**) Molecular graph of the [**4-COA**]$^+$ cation; density contours plotted in the RhH11C1 plane, BCPs (green) and RCPs (red); (**B**) Key BCP metrics and (**C**) donor-acceptor interactions associated with the Rh–H11C1 interaction; (**D**) NCI plot of the [**4-COA**][**BAr$^F_4$**] ion-pair; isosurface generated for s = 0.3 au and -0.07 < ρ < than 0.07 au); (**E**) Detail highlighting the region around Rh.

An interesting aspect of the NBO analysis of both [**2**]$^+$ and [**4-COA**]$^+$ is the degree of donation into σ^*_{C-H} from the *trans*-σ_{Rh-L} bonding orbitals (L = P2 or C32 respectively). In [**4-COA**]$^+$ this is supported by donation from the *cis*-σ_{Rh-H2} bonding orbital (see Figure 14). These interactions reflect the η^1-orientation of the C–H bonds in these species ([**2**]$^+$: $\angle RhHC_{calc}$(ave) = 138°; [**4-COA**]$^+$: $\angle RhHC_{calc}$ = 133°). Similar σ-donation has been identified with the onset of the C–H···Rh ('pregostic') interaction[93,94] and are consistent with the end-on approach of CH_4 in Bürgi-Dunitz trajectories[95] and of H_2 in oxidative addition reactions.[96,97]

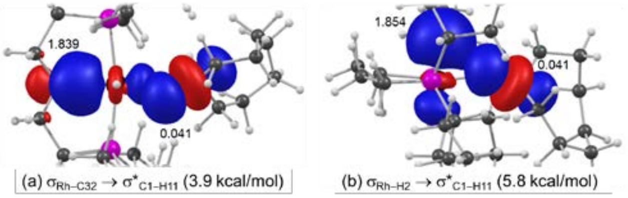

(a) $\sigma_{Rh-C32} \rightarrow \sigma^*_{C1-H11}$ (3.9 kcal/mol) (b) $\sigma_{Rh-H2} \rightarrow \sigma^*_{C1-H11}$ (5.8 kcal/mol)

Figure 14. NBO donor-acceptor pairs highlighting σ-donation from (a) the *trans*-Rh–C32 σ-bond and (b) the *cis*-Rh–H2 σ-bond into σ^*_{C-H}. NBO occupancies are also indicated.

3. CONCLUSIONS

The studies reported herein provide a demonstration of the power of Solid–State Organometallic Chemistry (SMOM–chem), and in particular single–crystal to single–crystal transformations to provide access to, and when combined with periodic DFT calculations, characterize a wide range of different sigma–alkane M···H–C coordination motifs by systematic variation of the ligand set. The complexes described present snapshots along a continuum of M···H–C interactions that would be very difficult to probe in σ–alkane complexes using solution techniques due to the instability of such systems combined with fluxionality between different M···H–C bonds that often results in a time–averaged structures in solution, even at very low tempertaures.[14] Thus with the NBA alkane ligand and simple, chelating, phosphines relativity strong bidentate chelating $\eta^2\eta^2$ motifs are observed, e.g. [**2–NBA**][**BAr$^F_4$**]. With a *trans* spanning C–H activated PCP pincer ligand, reduced access to the metal center results in unprecedented η^1 Rh(III)···H–C motifs being observed in the solid–state, e.g. [**4–COA**][**BAr$^F_4$**], a model for the early stages of C–H activation at metal centers. Finally, when the steric requirement of the phosphine and the alkane combine with the ability for the phosphine to engage in stabilizing intramolecular agostic interactions the alkane is expelled from the metal center, but remarkably stays encapsulated within the anion framework – providing baseline experimental structural data for a close – but essentially nonbonding – approach of an alkane with a metal center: viz. [**2**][**COA⊂BAr$^F_4$**]. Underpinning these remarkable structures is the stabilizing effect of the anion microenvironment, and in particular the role that intermolecular dispersion interactions play in stabilizing these alkane ligands within the binding pocket. Reflecting this, none of the complexes reported are stable in solution even at low temperature. The SMOM technique thus complements elegant low temperature in situ solution techniques for the synthesis and characterization of σ–alkane complexes.[29,31,81]

That such wide variations of alkane binding modes and structures are observed while a well–defined molecular environment is maintained in the solid–state provides an exemplar of a potentially tuneable, molecular heterogeneous system that can be precisely characterized. By using a core metal–ligand fragment, i.e. {Rh(diphosphine)}$^+$, it also offers a wide range of potential opportunities for transformations where variation of metal–ligand interactions are likely to influence rate, stability and selectivity in catalysis.[98] It will be interesting to see if this can be translated to productive C–H activation reactions of hydrocarbons using SMOM systems, and our efforts are currently focussed in this direction.

ASSOCIATED CONTENT

Supporting Information

Supporting information detailing the synthesis, structural characterization, solution and solid-state NMR experiments and computational studies. The Supporting Information is available free of charge on the ACS Publications website.

AUTHOR INFORMATION

Corresponding Author

Andrew Weller. andrew.weller@chem.ox.ac.uk
Stuart Macgregor , S.A.Macgregor@hw.ac.uk

ACKNOWLEDGMENT

SCG Chemicals Co. Ltd the EPSRC EP/M024210/1 and the Leverhulme Trust (RPG-2015-447). This work used the ARCHER UK National Supercomputing Service (http://www.archer.ac.uk); Professors J. Brown (Oxford) and

D. Heller (Leibniz-Institut für Katalyse) for helpful discussions

REFERENCES

(1) Hartwig, J. F. *Organotransition Metal Chemistry*; University Science Books: Sausalito, USA, 2010.

(2) van Leeuwen, P. W. N. M.; Chadwick, J. C. *Homogeneous Catalysis*; Wiley–VCH: Weinheim, 2011.

(3) van Leeuwen, P. W. N. M.; Kamer, P. C. J. Featuring Xantphos. *Cat. Sci. Tech.* **2018**, *8*, 26.

(4) Birkholz, M.-N.; Freixa, Z.; van Leeuwen, P. W. N. M. Bite angle effects of diphosphines in C-C and C-X bond forming cross coupling reactions. *Chem. Soc. Rev.* **2009**, *38*, 1099.

(5) Bilbrey, J. A.; Kazez, A. H.; Locklin, J.; Allen, W. D. Exact Ligand Solid Angles. *J. Chem. Theory Comput.* **2013**, *9*, 5734.

(6) Wilson, A. D.; Miller, A. J. M.; DuBois, D. L.; Labinger, J. A.; Bercaw, J. E. Thermodynamic Studies of $[H_2Rh(diphosphine)_2]^+$ and $[HRh(diphosphine)_2(CH_3CN)]^{2+}$ Complexes in Acetonitrile. *Inorg. Chem.* **2010**, *49*, 3918.

(7) Abdalla, J. A. B.; Caise, A.; Sindlinger, C. P.; Tirfoin, R.; Thompson, A. L.; Edwards, A. J.; Aldridge, S. Structural snapshots of concerted double E–H bond activation at a transition metal centre. *Nature Chem.* **2017**, *9*, 1256.

(8) Corma, A. Heterogeneous Catalysis: Understanding for Designing, and Designing for Applications. *Angew. Chem. Int. Ed.* **2016**, 55, 6112.

(9) Falkowski, J. M.; Sawano, T.; Zhang, T.; Tsun, G.; Chen, Y.; Lockard, J. V.; Lin, W. Privileged Phosphine-Based Metal–Organic Frameworks for Broad-Scope Asymmetric Catalysis. *J. Am. Chem. Soc.* **2014**, *136*, 5213.

(10) Bohnsack, A. M.; Ibarra, I. A.; Bakhmutov, V. I.; Lynch, V. M.; Humphrey, S. M. Rational Design of Porous Coordination Polymers Based on Bis(phosphine)MCl_2 Complexes That Exhibit High-Temperature H_2 Sorption and Chemical Reactivity. *J. Am. Chem. Soc.* **2013**, *135*, 16038.

(11) González-Gálvez, D.; Nolis, P.; Philippot, K.; Chaudret, B.; van Leeuwen, P. W. N. M. Phosphine-Stabilized Ruthenium Nanoparticles: The Effect of the Nature of the Ligand in Catalysis. *ACS Catal.* **2012**, *2*, 317.

(12) Thomas, J. M.; Raja, R. Exploiting Nanospace for Asymmetric Catalysis: Confinement of Immobilized, Single-Site Chiral Catalysts Enhances Enantioselectivity. *Acc. Chem. Res.* **2008**, *41*, 708.

(13) Copéret, C.; Comas-Vives, A.; Conley, M. P.; Estes, D. P.; Fedorov, A.; Mougel, V.; Nagae, H.; Núñez-Zarur, F.; Zhizhko, P. A. Surface Organometallic and Coordination Chemistry toward Single-Site Heterogeneous Catalysts: Strategies, Methods, Structures, and Activities. *Chem. Rev.* **2016**, *116*, 323.

(14) Weller, A. S.; Chadwick, F. M.; McKay, A. I. In *Adv. Organomet. Chem.*; Pérez, P. J., Ed.; Academic Press, 2016; Vol. 66.

(15) Hall, C.; Perutz, R. N. Transition Metal Alkane Complexes. *Chem. Rev.* **1996**, *96*, 3125.

(16) Young, R. D. Characterisation of Alkane σ - Complexes. *Chem. Eur. J.* **2014**, *20*, 12704.

(17) Pike, S. D.; Thompson, A. L.; Algarra, A. G.; Apperley, D. C.; Macgregor, S. A.; Weller, A. S. Synthesis and Characterization of a Rhodium(I) σ-Alkane Complex in the Solid State. *Science* **2012**, *337*, 1648.

(18) Pike, S. D.; Chadwick, F. M.; Rees, N. H.; Scott, M. P.; Weller, A. S.; Krämer, T.; Macgregor, S. A. Solid-State Synthesis and Characterization of σ-Alkane Complexes, $[Rh(L_2)(\eta^2,\eta^2\text{-}C_7H_{12})][BAr^F_4]$ (L_2 = Bidentate Chelating Phosphine). *J. Am. Chem. Soc.* **2015**, *137*, 820.

(19) McKay, A. I.; Krämer, T.; Rees, N. H.; Thompson, A. L.; Christensen, K. E.; Macgregor, S. A.; Weller, A. S. Formation of a σ-alkane Complex and a Molecular Rearrangement in the Solid-State: $[Rh(Cyp_2PCH_2CH_2PCyp_2)(\eta^2{:}\eta^2\text{-}C_7H_{12})][BAr^F_4]$. *Organometallics* **2017**, *36*, 22.

(20) McKay, A. I.; Martínez-Martínez, A. J.; Griffiths, H. J.; Rees, N. H.; Waters, J. B.; Weller, A. S.; Krämer, T.; Macgregor, S. A. Controlling Structure and Reactivity in Cationic Solid-State Molecular Organometallic Systems Using Anion Templating. *Organometallics* **2018**, *in the press DOI: 10.1021/acs.organomet.8b00215*.

(21) Kubas, G. J. *Metal Dihydrogen and σ-Bond Complexes*; Kluwer: New York, 2001.

(22) Green, J. C.; Green, M. L. H.; Parkin, G. The occurrence and representation of three-centre two-electron bonds in covalent inorganic compounds. *Chem. Commun.* **2012**, *48*, 11481.

(23) Bergman, R. G. Organometallic chemistry: C-H activation. *Nature* **2007**, *446*, 391.

(24) Goldberg, K. I.; Goldman, A. S. Large-Scale Selective Functionalization of Alkanes. *Acc. Chem. Res.* **2017**, *50*, 620.

(25) *Alkane C-H Activation by Single-Site Metal Catalysis*; Perez, P. J., Ed.; Spinger: Dordrecht, 2012; Vol. 38.

(26) Chadwick, F. M.; Krämer, T.; Gutmann, T.; Rees, N. H.; Thompson, A. L.; Edwards, A. J.; Buntkowsky, G.; Macgregor, S. A.; Weller, A. S. Selective C–H Activation at a Molecular Rhodium Sigma-Alkane Complex by Solid/Gas Single-Crystal to Single-Crystal H/D Exchange. *J. Am. Chem. Soc.* **2016**, *138*, 13369.

(27) Geftakis, S.; Ball, G. E. Direct observation of a transition metal alkane complex, $CpRe(CO)_2$(cyclopentane), using NMR spectroscopy. *J. Am. Chem. Soc.* **1998**, *120*, 9953.

(28) Bernskoetter, W. H.; Schauer, C. K.; Goldberg, K. I.; Brookhart, M. Characterization of a Rhodium(I) -Methane Complex in Solution. *Science* **2009**, *326*, 553.

(29) Calladine, J. A.; Duckett, S. B.; George, M. W.; Matthews, S. L.; Perutz, R. N.; Torres, O.; Vuong, K. Q. Manganese Alkane Complexes: An IR and NMR Spectroscopic Investigation. *J. Am. Chem. Soc.* **2011**, *133*, 2303.

(30) Walter, M. D.; White, P. S.; Schauer, C. K.; Brookhart, M. Stability and Dynamic Processes in 16VE Iridium(III) Ethyl Hydride and Rhodium(I) σ-Ethane Complexes: Experimental and Computational Studies. *J. Am. Chem. Soc.* **2013**, *135*, 15933.

(31) Yau, H. M.; McKay, A. I.; Hesse, H.; Xu, R.; He, M.; Holt, C. E.; Ball, G. E. Observation of Cationic Transition Metal-Alkane Complexes with Moderate Stability in Hydrofluorocarbon Solution. *J. Am. Chem. Soc.* **2016**, *138*, 281.

(32) Petrosko, S. H.; Johnson, R.; White, H.; Mirkin, C. A. Nanoreactors: Small Spaces, Big Implications in Chemistry. *J. Am. Chem. Soc.* **2016**, *138*, 7443.

(33) Chadwick, F. M.; McKay, A. I.; Martinez-Martinez, A. J.; Rees, N. H.; Kramer, T.; Macgregor, S. A.; Weller, A. S. Solid-state molecular organometallic chemistry. Single-crystal to single-crystal reactivity and catalysis with light hydrocarbon substrates. *Chem. Sci.* **2017**, *8*, 6014.

(34) Thomas, J. M. *Design and Applications of Single-Site Heterogeneous Catalysts*; Imperial College Press: London, 2012.

(35) Gonzalez, M. I.; Mason, J. A.; Bloch, E. D.; Teat, S. J.; Gagnon, K. J.; Morrison, G. Y.; Queen, W. L.; Long, J. R. Structural characterization of framework-gas interactions in the metal-organic framework Co_2(dobdc) by in situ single-crystal X-ray diffraction. *Chem. Sci.* **2017**, *8*, 4387.

(36) Li, Z.; Peters, A. W.; Bernales, V.; Ortuño, M. A.; Schweitzer, N. M.; DeStefano, M. R.; Gallington, L. C.; Platero-Prats, A. E.; Chapman, K. W.; Cramer, C. J. et al. Metal–Organic Framework Supported Cobalt Catalysts for the Oxidative Dehydrogenation of Propane at Low Temperature. *ACS Cent. Sci.* **2017**, *3*, 31.

(37) Burgun, A.; Coghlan Campbell, J.; Huang David, M.; Chen, W.; Horike, S.; Kitagawa, S.; Alvino Jason, F.; Metha Gregory, F.; Sumby Christopher, J.; Doonan Christian, J. Mapping ‐ Out Catalytic Processes in a Metal – Organic Framework with Single ‐ Crystal X ‐ ray Crystallography. *Angew. Chem. Int. Ed.* **2017,** *129*, 8532.

(38) Pike, S. D.; Crimmin, M. R.; Chaplin, A. B. Organometallic chemistry using partially fluorinated benzenes. *Chem. Commun.* **2017,** 53, 3615.

(39) See Supporting Materials

(40) Meißner, A.; Alberico, E.; Drexler, H.-J.; Baumann, W.; Heller, D. Rhodium diphosphine complexes: a case study for catalyst activation and deactivation. *Cat. Sci. Tech.* **2014,** *4*, 3409.

(41) Heller, D.; De Vries, A. H.; De Vries, J. G. In *The Handbook of Homogeneous Hydrogenation*; Wiley–VCH: Weinheim, 2007.

(42) Green, M. L. H.; Parkin, G. In *The Chemical Bond III: 100 years old and getting stronger*; Mingos, D. M. P., Ed.; Springer International Publishing: Cham, 2017, 206.

(43) Smart, K. A.; Grellier, M.; Coppel, Y.; Vendier, L.; Mason, S. A.; Capelli, S. C.; Albinati, A.; Montiel-Palma, V.; Muñoz-Hernández, M. A.; Sabo-Etienne, S. Nature of Si–H Interactions in a Series of Ruthenium Silazane Complexes Using Multinuclear Solid-State NMR and Neutron Diffraction. *Inorg. Chem.* **2014,** 53, 1156.

(44) In the 298 K $^1H/^{13}C$ HETCOR additional cross peaks are seen between signals $\delta(^1H)$ 0 to –1 and $\delta^{13}C$ 17 to 20. Close inspection of the seconary interactions in **[3–NBA][BAr$^F{}_4$]** reveals a number of C–H bonds in the phosphine that lie over the centers of anion aryl rings (H···C6 centroid 2.82 – 2.94 Å), and are thus likely to experience ring current effects. In addition, the NBA fragment is likey undergoing a C_2 rotation in the solid–state on the NMR timescale at 298 K, as reported for **[1–NBA][BAr$^F{}_4$]**.

(45) Douglas, T. M.; Molinos, E.; Brayshaw, S. K.; Weller, A. S. Rhodium Phosphine Olefin Complexes of the Weakly Coordinating Anions $[BAr^F{}_4]^-$ and $[1\text{-closo-}CB_{11}H_6Br_6]^-$. Kinetic versus Thermodynamic Factors in Anion Coordination and Complex Reactivity. *Organometallics* **2007,** *26*, 463.

(46) Chaplin, A. B. Rhodium(I) Complexes of the Conformationally Rigid IBioxMe$_4$ Ligand: Isolation of a Stable Low-Coordinate T-Shaped Complex. *Organometallics* **2014,** *33*, 624.

(47) Ingleson, M.; Fan, H.; Pink, M.; Tomaszewski, J.; Caulton, K. G. Three-Coordinate Co(I) Provides Access to Unsaturated Dihydrido-Co(III) and Seven-Coordinate Co(V). *J. Am. Chem. Soc.* **2006,** *128*, 1804.

(48) Brookhart, M.; Green, M. L. H.; Parkin, G. Agostic interactions in transition metal compounds. *Proc. Nat. Acad. (USA)* **2007,** *104*, 6908.

(49) Knighton R. C.; Emerson ‐ King, J.; Rourke Jonathan, P.; Ohlin, C. A.; Chaplin Adrian, B. Solution, Solid ‐ State, and Computational Analysis of Agostic Interactions in a Coherent Set of Low ‐ Coordinate Rhodium(III) and Iridium(III) Complexes. *Chem. Eur. J.* **2018,** *24*, 4927.

(50) Sewell, L. J.; Chaplin, A. B.; Abdalla, J. A. B.; Weller, A. S. Reversible C-H activation of a $P^tBu^iBu_2$ ligand to reveal a masked 12 electron $[Rh(PR_3)_2]^+$ cation. *Dalton Trans.* **2010,** *39*, 7437.

(51) NCI plots on **[2]**$^+$ suggest significant intramolecular dispersion stablisation between the Cy groups not involved in the agostic interactions.

(52) van der Eide Edwin, F.; Yang, P.; Bullock, R. M. Isolation of Two Agostic Isomers of an Organometallic Cation: Different Structures and Colors. *Angew. Chem. Int. Ed.* **2013,** *52*, 10190.

(53) Meier S. C.; Holz, A.; Kulenkampff, J.; Schmidt, A.; Kratzert, D.; Himmel, D.; Schmitz, D.; Scheidt, E.-W.; Scherer, W.; Bülow, C. et al. Access to the Bis-benzene Cobalt(I) Sandwich Cation and its Derivatives: Synthons for a "Naked" Cobalt(I) Source? *Angew. Chem. Int. Ed.* **2018,** *54*, 9310.

(54) Douglas, T. M.; Chaplin, A. B.; Weller, A. S. Dihydrogen Loss from a 14-Electron Rhodium(III) Bis-Phosphine Dihydride To Give a Rhodium(I) Complex That Undergoes Oxidative Addition with Aryl Chlorides. *Organometallics* **2008,** *27*, 2918.

(55) Kohyama, Y.; Murase, T.; Fujita, M. Metal–Organic Proximity in a Synthetic Pocket. *J. Am. Chem. Soc.* **2014,** *136*, 2966.

(56) Ajami, D.; Rebek Jr, J. Compressed alkanes in reversible encapsulation complexes. *Nature Chem.* **2009,** *1*, 87.

(57) Pakes, P. W.; Rounds, T. C.; Strauss, H. L. Conformations of cyclooctane and some related oxocanes. *J. Phys. Chem.* **1981,** *85*, 2469.

(58) Castro-Rodriguez, I.; Nakai, H.; Gantzel, P.; Zakharov, L. N.; Rheingold, A. L.; Meyer, K. Evidence for Alkane Coordination to an Electron-Rich Uranium Center. *J. Am. Chem. Soc.* **2003,** *125*, 15734.

(59) Arnold P. L.; Prescimone, A.; Farnaby Joy, H.; Mansell Stephen, M.; Parsons, S.; Kaltsoyannis, N. Characterizing Pressure ‐ Induced Uranium C···H Agostic Bonds. *Angew. Chem. Int. Ed.* **2015,** *54*, 6735.

(60) Braga, D. Dynamical processes in crystalline organometallic complexes. *Chem. Rev.* **1992,** *92*, 633.

(61) Chaplin, A. B.; Green, J. C.; Weller, A. S. C–C Activation in the Solid State in an Organometallic σ-Complex. *J. Am. Chem. Soc.* **2011,** *133*, 13162.

(62) Tahir Mohamed, I. M.; Rees Nicholas, H.; Heyes Stephen, J.; Cowley Andrew, R.; Prout, K. Discrimination of chiral guests by chiral channels: Variable temperature studies by SXRD and solid state 13C NMR of the deoxycholic acid complexes of camphorquinone and endo ‐ 3 ‐ bromocamphor. *Chirality* **2008,** *20*, 863.

(63) Torres-Huerta, A.; Rodríguez-Molina, B.; Höpfl, H.; Garcia-Garibay, M. A. Synthesis and Solid-State Characterization of Self-Assembled Macrocyclic Molecular Rotors of Bis(dithiocarbamate) Ligands with Diorganotin(IV). *Organometallics* **2014,** *33*, 354.

(64) Lattice mobilty of COA formed from solid/gas reaction between $[Ir(PPh_3)_2(COD)][PW_{12}O_{40}]$ and D_2 has been proposed on the basis of line shape analysis of ^2H SSNMR spectrum. Siedle, A. R.; Newmark, R. A.; Sahyun, M. R. V.; Lyon, P. A.; Hunt, S. L.; Skarjune R. P. Solid-state Chemistry of Molecular Metal Oxide Clusters. Multiple, Sequential C-H Activation Processes in the Hydrogenation of Coordinated Cyclooctene. Lattice Mobility of Small Organic Molecules. *J. Am. Chem. Soc.* **1989,** *111*, 8346

(65) Alvarez, S. A cartography of the van der Waals territories. *Dalton Trans.* **2013,** *42*, 8617.

(66) Crocker, C.; Errington, R. J.; McDonald, W. S.; Odell, K. J.; Shaw, B. L.; Goodfellow, R. J. Rapid reversible fission of a C-H bond in a metal complex: X-ray crystal structure of $[RhHCl(Bu^t{}_2PCH_2CH_2CHCH_2CH_2PBu^t{}_2)]$. *J. Chem. Soc., Chem. Commun.* **1979**, 498.

(67) Brown, J. M.; Chaloner, P. A.; Kent, A. G.; Murrer, B. A.; Nicholson, P. N.; Parker, D.; Sidebottom, P. J. The mechanism of asymmetric homogeneous hydrogenation. Solvent complexes and dihydrides from rhodium diphosphine precursors. *J. Organomet. Chem.* **1981,** *216*, 263.

(68) McLoughlin, M. A.; Flesher, R. J.; Kaska, W. C.; Mayer, H. A. Synthesis and Reactivity of $[IrH_2(^tBu_2P)CH_2CH_2CHCH_2CH_2P(^tBu_2)]$, a Dynamic Iridium Polyhydride Complex. *Organometallics* **1994,** *13*, 3816.

(69) Empsall, H. D.; Hyde, E. M.; Markham, R.; McDonald, W. S.; Norton, M. C.; Shaw, B. L.; Weeks, B. Synthesis and X-ray structure of an unusual iridium ylide or carbene complex. *J. Chem. Soc., Chem. Commun.* **1977**, 589.

(70) Baratta, W.; Mealli, C.; Herdtweck, E.; Ienco, A.; Mason, S. A.; Rigo, P. Nonclassical vs Classical Metal···H_3C–C Interactions: Accurate Characterization of a 14-Electron Ruthenium(II) System by Neutron Diffraction, Database Analysis, Solution Dynamics, and DFT Studies. *J. Am. Chem. Soc.* **2004,** *126*, 5549.

(71) Weng, W.; Guo, C.; Moura, C.; Yang, L.; Foxman, B. M.; Ozerov, O. V. Competitive Activation of N–C and C–H Bonds of the PNP Framework by Monovalent Rhodium and Iridium. *Organometallics* **2005,** *24*, 3487.

(72) Pregosin, P. S. *NMR in Organometallic Chemistry*; Wiley-VCH: Weinheim, 2012.

(73) Taw, F. L.; Mellows, H.; White, P. S.; Hollander, F. J.; Bergman, R. G.; Brookhart, M.; Heinekey, D. M. Synthesis and Investigation of $[Cp^*(PMe_3)Rh(H)(H_2)]^+$ and Its Partially Deuterated and Tritiated Isotopomers: Evidence for a Hydride/Dihydrogen Structure. *J. Am. Chem. Soc.* **2002,** *124*, 5100.

(74) Adams, G. M.; Chadwick, F. M.; Pike, S. D.; Weller, A. S. A CH_2Cl_2 complex of a $[Rh(pincer)]^+$ cation. *Dalton Trans.* **2015,** *44*, 6340.

(75) Scott, N. M.; Dorta, R.; Stevens, E. D.; Correa, A.; Cavallo, L.; Nolan, S. P. Interaction of a Bulky N-Heterocyclic Carbene Ligand with Rh(I) and Ir(I). Double C–H Activation and Isolation of Bare 14-Electron Rh(III) and Ir(III) Complexes. *J. Am. Chem. Soc.* **2005,** *127*, 3516.

(76) Häller, L. J. L.; Mas-Marzá, E.; Cybulski, M. K.; Sanguramath, R. A.; Macgregor, S. A.; Mahon, M. F.; Raynaud, C.; Russell, C. A.; Whittlesey, M. K. Computation provides chemical insight into the diverse hydride NMR chemical shifts of $[Ru(NHC)_4(L)H]^{0/+}$ species (NHC = N-heterocyclic carbene; L = vacant, H_2, N_2, CO, MeCN, O_2, P_4, SO_2, H^-, F^- and Cl^-) and their $[Ru(R_2PCH_2CH_2PR_2)_2(L)H]^+$ congeners. *Dalton Trans.* **2017,** *46*, 2861.

(77) Huang, D.; Huffman, J. C.; Bollinger, J. C.; Eisenstein, O.; Caulton, K. G. The First η^2-CH_2Cl_2 Adduct of Ru(II):$[RuH(\eta^2\text{-}CH_2Cl_2)(CO)(P^tBu_2Me)_2][BAr'_4]$ (Ar' = 3,5-$C_6H_3(CF_3)_2$) and Its $RuH(CO)(P^tBu_2Me)_2{}^+$ Precursor. *J. Am. Chem. Soc.* **1997,** *119*, 7398.

(78) Chadwick, F. M.; Rees Nicholas, H.; Weller Andrew, S.; Krämer, T.; Iannuzzi, M.; Macgregor Stuart, A. A Rhodium–Pentane Sigma - Alkane Complex: Characterization in the Solid State by Experimental and Computational Techniques. *Angew. Chem. Int. Ed.* **2016,** *128*, 3741.

(79) Pitts, A. L.; Wriglesworth, A.; Sun, X.-Z.; Calladine, J. A.; Zarić, S. D.; George, M. W.; Hall, M. B. Carbon–Hydrogen Activation of Cycloalkanes by Cyclopentadienylcarbonylrhodium—A Lifetime Enigma. *J. Am. Chem. Soc.* **2014,** *136*, 8614.

(80) Guan, J.; Wriglesworth, A.; Sun, X. Z.; Brothers, E. N.; Zarić, S. D.; Evans, M. E.; Jones, W. D.; Towrie, M.; Hall, M. B.; George, M. W. Probing the Carbon–Hydrogen Activation of Alkanes Following Photolysis of Tp'Rh(CNR)(carbodiimide): A Computational and Time-Resolved Infrared Spectroscopic Study. *J. Am. Chem. Soc.* **2018,** *140*, 1842.

(81) Asplund, M. C.; Snee, P. T.; Yeston, J. S.; Wilkens, M. J.; Payne, C. K.; Yang, H.; Kotz, K. T.; Frei, H.; Bergman, R. G.; Harris, C. B. Ultrafast UV Pump/IR Probe Studies of C–H Activation in Linear, Cyclic, and Aryl Hydrocarbons. *J. Am. Chem. Soc.* **2002,** *124*, 10605.

(82) Balcells, D.; Clot, E.; Eisenstein, O. C—H Bond Activation in Transition Metal Species from a Computational Perspective. *Chem. Rev.* **2010,** *110*, 749.

(83) Yang, J.; White, P. S.; Schauer, C. K.; Brookhart, M. Structural and Spectroscopic Characterization of an Unprecedented Cationic Transition-Metal η^1-Silane Complex. *Angew. Chem. Int. Ed.* **2008,** *47*, 4141.

(84) Johnson, H. C.; McMullin, C. L.; Pike, S. D.; Macgregor, S. A.; Weller, A. S. Dehydrogenative Boron Homocoupling of an Amine-Borane. *Angew. Chem. Int. Ed.* **2013,** *52*, 9776.

(85) Zhu, D.; Sharma, A. Z.; Wiebe, C. R.; Budzelaar, P. H. M. Rhodium(II) dimers without metal-metal bonds. *Dalton Trans.* **2015,** *44*, 13460.

(86) A previous study on **[1-NBA][BAr$^F_4$]** used a slightly different protocol (ref. 18) and so this system was recomputed with the current approach for consistency. Very similar data to our previous study were obtained.

(87) Contreras-García, J.; Johnson, E. R.; Keinan, S.; Chaudret, R.; Piquemal, J.-P.; Beratan, D. N.; Yang, W. NCIPLOT: A Program for Plotting Noncovalent Interaction Regions. *J. Chem. Theory Comput.* **2011,** *7*, 625.

(88) Narth, C.; Maroun, Z.; Boto, R. A.; Chaudret, R.; Bonnet, M.-L.; Piquemal, J.-P.; Contreras-García, J. In *Applications of Topological Methods in Molecular Chemistry*; Chauvin, R.;Lepetit, C.;Silvi, B.;Alikhani, E., Eds.; Springer International Publishing: Cham, 2016.

(89) Lane, J. R.; Contreras-García, J.; Piquemal, J.-P.; Miller, B. J.; Kjaergaard, H. G. Are Bond Critical Points Really Critical for Hydrogen Bonding? *J. Chem. Theory Comput.* **2013,** *9*, 3263.

(90) It has been recently suggested that dispersion may also contribute to intramolecular C–H···M interactions. See: Lu, Q.; Neese, F.; Bistoni, G. Formation of Agostic Structures Driven by London Dispersion, Angew. Chem. Int. Ed. **2018**, 57, 4760-4764.

(91) Additional weak Rh···H–C interactions with similar BCPs metrics were also computed involving cyclohexyl C-H bonds in **[3-NBA]**$^+$ and **[2]**$^+$. See Supporting Materials.

(92) The COA sits within in a square-pyramidal array of BAr$^F_4$ anions (cf. Figure 3) and Figure 13 shows the 'axial' $[BAr^F_4]^-$ anion. Stabilizing non-covalent interactions are also seen to the four basal $[BAr^F_4]^-$ anions but these are less significant (see Figure S91, Supporting Materials).

(93) Scherer, W.; Dunbar, A. C.; Barquera-Lozada, J. E.; Schmitz, D.; Eickerling, G.; Kratzert, D.; Stalke, D.; Lanza, A.; Macchi, P.; Casati, N. P. M.et al. Anagostic Interactions under Pressure: Attractive or Repulsive? *Angew. Chem. Int. Ed.* **2015,** *54*, 2505.

(94) Nielson, A. J.; Harrison, J. A.; Sajjad, M. A.; Schwerdtfeger, P. Electronic and Steric Manipulation of the Preagostic Interaction in Isoquinoline Complexes of RhI. *Eur. J. Inorg. Chem.* **2017,** 2255.

(95) Crabtree, R. H. The organometallic chemistry of alkanes. *Chem. Rev.* **1985,** *85*, 245.

(96) Macgregor, S. A.; Eisenstein, O.; Whittlesey, M. K.; Perutz, R. N. A theoretical study of $[M(PH_3)_4]$ (M = Ru or Fe), models for the highly reactive d^8 intermediates $[M(dmpe)_2]$ (dmpe = $Me_2PCH_2CH_2PMe_2$). Zero activation energies for addition of CO and oxidative addition of H_2. *J. Chem. Soc., Dalton Trans.***1998**, 291.

(97) Similar σ-donation is also seen in **[2-NBA]**$^+$ but this is weak (1.1 kcal/mol, from cis-σ_{RhP_2}) reflecting the tighter RhHC angle (102º).

(98) *Applied Homogeneous Catalysis with Organometallic Compounds*; Boy Cornils; Herrmann, W. A.; Beller, M.; Paciello, R., Eds.; Wiley–VCH: Wieheim, 2017.

For Toc

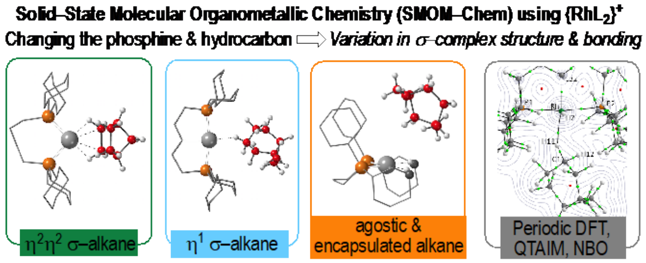
Solid–State Molecular Organometallic Chemistry (SMOM–Chem) using $\{RhL_2\}^+$
Changing the phosphine & hydrocarbon ⟹ *Variation in σ–complex structure & bonding*
$\eta^2\eta^2$ σ–alkane
η^1 σ–alkane
agostic & encapsulated alkane
Periodic DFT, QTAIM, NBO
